CHEMISTRY OF MATERIALS

Open Access

pubs.acs.org/cm

Article

Carbonate Chemistry Regulates Ion Transport from Polymer–Calcium Condensates for Bioinspired Calcification

Debojit Paul, Oliver Jeske, Oksana Yanshyna, Liat Avram, Denis Gebauer, and Assaf Gal*

Cite This: *Chem. Mater.* 2026, 38, 950–960

Read Online

ACCESS | Metrics & More | Article Recommendations | Supporting Information

ABSTRACT: Amorphous calcium carbonate phases are common intermediates in multistep crystallization processes. In many cases, it was shown that these dense and liquid-like phases function as transient metastable precursors that transform into mature crystalline phases. However, some biological systems consist of inorganic condensates that serve only as ion carriers and dissolve prior to the formation of the mineral. In this work, we study the chemical conditions that regulate the release of calcium ions from polymer condensates toward the formation of calcium carbonate. It is shown that the presence of bicarbonate ions tunes the stability of biogenic and bioinspired polymer–Ca condensates. In specific conditions of the carbonate system, condensate dissolution is induced, affecting calcium carbonate supersaturation and crystallization kinetics. This behavior recapitulates observations on the roles of such condensates in vivo, suggesting that bicarbonate ions indirectly affect mineralization by turning inorganic condensates from mineral precursors into sacrificial ion pools.

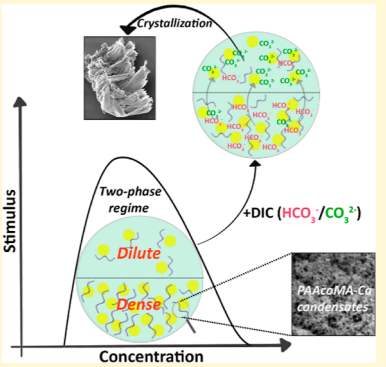

INTRODUCTION

Biologically formed calcium carbonate minerals are characterized by superior properties relative to analogous synthetic materials.[1,2] This is usually the result of macromolecules that are incorporated in and around the crystals and contribute to the mechanical, structural, and hierarchical complexities of biominerals.[3−6] More specifically, it is well established that negatively charged macromolecules, such as proteins and polysaccharides, are intimately associated with biological processes of calcium carbonate precipitation.[7−11] They can form stereochemical templates to guide nucleation and alter crystal growth, or they can function indirectly as process-directing agents that stabilize amorphous phases and can drive the crystallization process into multistep, also known as "nonclassical" routes.[12−14] However, the chemical processes by which these macromolecules affect crystallization are not well understood.

It is usually assumed that the major influence of these macromolecules is via interactions with the calcium carbonate phases, for example, via kinetically inhibiting calcium carbonate crystallization or driving polymorph control toward a uniform outcome.[9,15−17] In vitro, these interactions led to the concept of polymer-induced liquid precursors (PILP).[18] An additional emerging concept is the formation of liquid-like dense phases, or coacervates, due to the electrostatic interactions between the charged macromolecules and the inorganic ions.[19−25] Such polymer–ion condensates were shown to form via the phase separation of poly(acrylic acid) (PAA) and calcium ions, followed by their conversion into nonstoichiometric amorphous calcium carbonate (ACC) phases that crystallize to calcite.[26] Altogether, the PILP and dense polymer phase pathways might well explain the abundance of biominerals that form via sequential transformations of amorphous phases until the mature phase is achieved. Indeed, in vivo evidence accumulates to the role of dense mineral phases as precursors for crystalline materials.[27−31]

Nevertheless, not all biominerals form via an amorphous precursor and some of them, for example, coccoliths, demonstrate all the characteristics of a one-step, monomer-by-monomer growth.[32−34] An interesting feature is that, also in these systems, the crystallization process is associated with similar macromolecules and condensates.[35] In recent years, an alternative role for such inorganic condensates was proposed as regulators of the chemical environment, creating a localized Ca-rich environment that prefers crystallization. In this process, the polymer–Ca condensates function as a preceding step for calcium carbonate formation. This was demonstrated in coccoliths, arrays of calcite crystals formed by unicellular algae on the periphery of an organic base plate. Coccolith-associated polysaccharides (CAPs) were shown to react with soluble calcium ions and form a dense phase at the sites destined for crystal growth.[36−38] This phenomenon was mimicked by a specific synthetic polymer, poly(acrylic co-maleic acid) (PAAcoMA).[39] However, calcite crystals never

Received: November 20, 2025
Revised: December 30, 2025
Accepted: December 30, 2025
Published: January 13, 2026

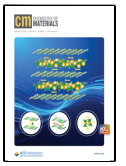

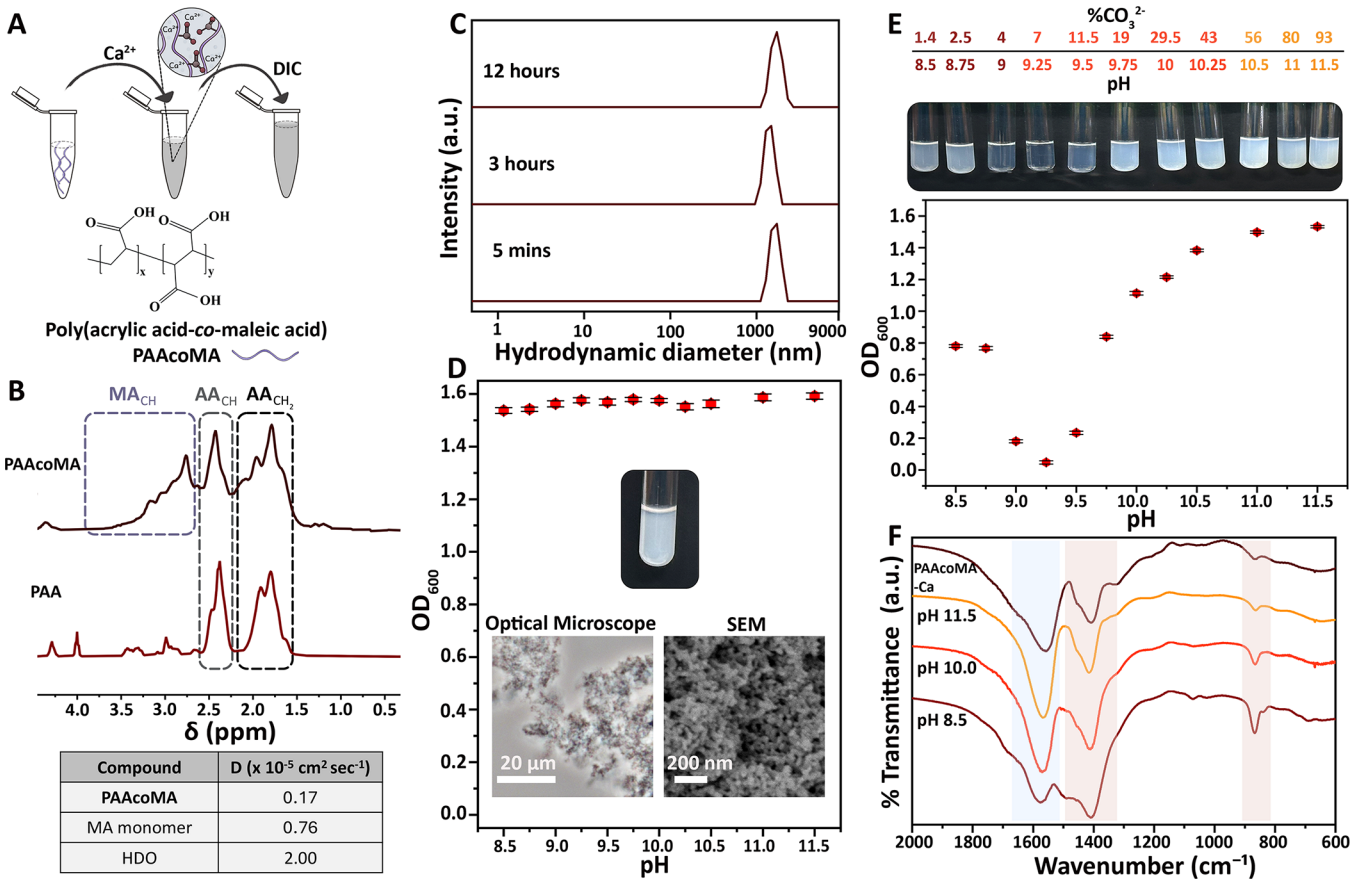

Figure 1. (A) The chemical formula of PAAcoMA, and the two-step experiment where first calcium is added to the polymer solution to induce coacervation, followed by DIC addition. (B) Partial ^{1}H 1D diffusion NMR spectra of PAA and PAAcoMA. See Figure S1 for deconvolution data of the standard NMR spectra. The table presents the diffusion coefficients of PAAcoMA, along with those of the MA monomer and HDO, as determined by diffusion NMR. See also Figure S2. (C) PAAcoMA−Ca condensate particle sizes determined by DLS at different time intervals (pH 8.75). (D) Turbidity in mixtures of 50 mM PAAcoMA and 25 mM $CaCl_2$ at various pH values. Insets show visual appearance of the mixture, optical microscopy, and an scanning electron microscope (SEM) image of dried precipitates. (E) Images and turbidity measurements of the same mixtures in (D) directly after adding a DIC solution with 20 mM $[CO_3^{2-}]$ at the same pH. The table at the top shows the carbonate percentage (the rest are bicarbonate ions). (F) FTIR spectra of washed and dried precipitates that formed at several pH values after the addition of the DIC. The precipitates in the basic pH are similar to the DIC-free spectrum (dominant polymer peak highlighted in blue), while carbonate peaks (in pink) are more prominent in the lower pH values. See full pH range in Figure S5.

grew from these dense phases in vitro, and in vivo observations suggest that the biogenic condensates dissolve next to the growing crystals,[28,29] thereby providing them with soluble building blocks. These observations point to pathways in which calcium−polymer condensates are not direct precursors for calcium carbonate but rather serve as high-capacity ion carriers.

Here, we study in vitro the behavior of PAAcoMA−Ca condensates in the presence of carbonate species across different pH values. We show that PAAcoMA forms solid-like condensates that do not transform into transient ACC. Nevertheless, the presence of carbonate in the surrounding dilute phase can induce the dissolution of the condensates in a concentration- and pH-dependent manner. This changes the chemical conditions in the dilute phase, which is manifested in different kinetics of the calcite crystallization process.

RESULTS

The PAAcoMA used in the experiments consists of an approximately 1:1 ratio of acrylic to maleic acid residues and a minor fraction of monomers as determined by NMR analyses (Figures 1A,B, S1 and S2), and a molecular weight of ∼3000 g mol^{-1}, as extracted from diffusion NMR. We tested the interactions between PAAcoMA and Ca^{2+} ions under high concentrations that are relevant to biomineralization.[40] The chosen concentrations were in the mM range, 50 mM of the carboxylic acid residues of the polymer, and 25 mM Ca^{2+}. Indeed, upon mixing the polymer and calcium solutions, instantaneous turbidity appears as a result of polymer−Ca coacervation. Turbidity was not affected by the ionic strength of the solution (Figure S3). The turbid solutions were characterized by dynamic light scattering (DLS), showing the presence of particles that did not coalesce with time (Figure 1C). The turbidity values were mostly invariant to pH in the range of 8.5−11.5 (Figure 1D), which is expected since the polymer is mostly deprotonated in this pH range (Figure S4). In contrast to the liquid behavior of the previously studied PAA−Ca condensates,[26] the solid-like nature of the PAAcoMA−Ca condensates was evidenced by its nanogranular morphology (Figure 1D, inset).

In the next step, we added a carbonate solution to the PAAcoMA−Ca condensate solution. We scanned the entire pH range of 8.5−11.5, as it is unclear what the relevant physiological pH is. Since pH affects the speciation of the

https://doi.org/10.1021/acs.chemmater.5c03138
Chem. Mater. 2026, 38, 950−960

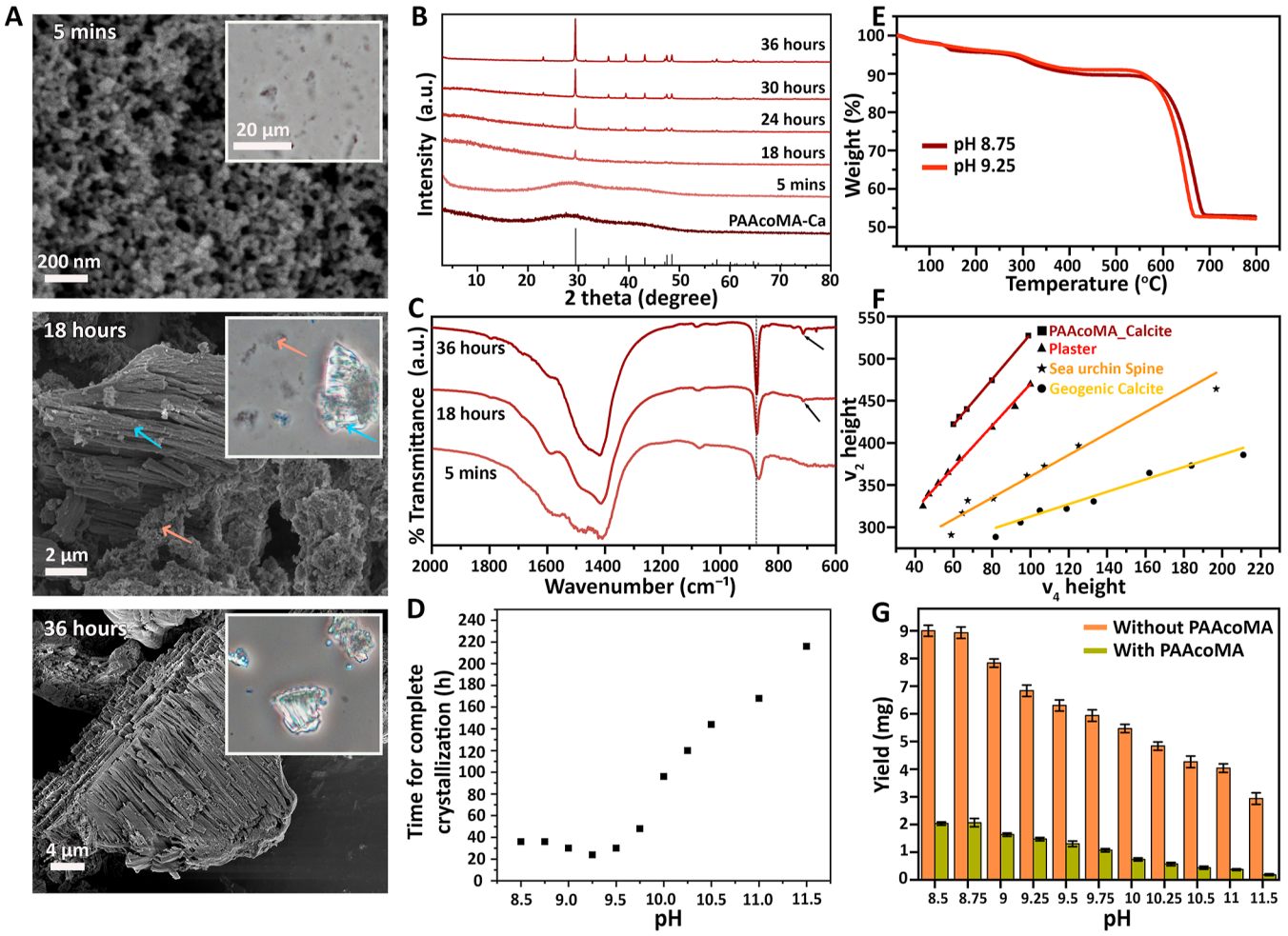

Figure 2. (A) Representative SEM images (insets showing optical microscopy images) of calcite crystallization in PAAcoMA−Ca system in three time points after addition of a DIC solution at pH 8.75. After 5 min, only coacervates are seen; after 18 h, crystals can also be detected; until crystallization is complete after 36 h. (B) PXRD patterns of the same samples at different time intervals showing the evolution of calcite from the PAAcoMA−Ca condensate upon DIC addition. XRD reflections of calcite standard are presented at the bottom. (C) FTIR spectra of the same samples as in (A) at three different time intervals. (D) The time of complete crystallization (where no coacervates can be detected) as a function of the reaction pH. (E) TGA traces of the crystals that formed under two pH conditions. (F) Grinding curves of four calcite samples.[41] The slope of the crystals formed from the PAAcoMA−Ca coacervates is similar to disordered plaster crystals. (G) The yield of the precipitation reaction at various pH values is reported as mass of the forming crystals.

dissolved inorganic carbon (DIC) species, we decided to keep $[CO_3^{2-}]$ at 20 mM, as this will keep a nominally constant saturation level with respect to calcium carbonate across all experiments. In practice, the PAAcoMA−Ca condensates were prepared by mixing two mother solutions adjusted to the chosen pH, after which a DIC solution at the constant $[CO_3^{2-}]$ and pH, but with varied $[HCO_3^-]$ concentrations, was added (Figure 1E). The ionic strength of all DIC solutions was kept constant by the addition of the relevant amount of NaCl.

Unexpectedly, the effect of mixing the PAAcoMA−Ca condensates with the DIC solution was pH-dependent. At the basic conditions of pH 11.5, where carbonate is the dominant species, no change in turbidity was observed, but at lower pH values, there was a clear loss of turbidity over a few seconds until complete clearing of the solution at pH 9.25 (Figure 1E). At even lower pH values, where bicarbonate is the dominant species, turbidity still decreased but only to about half of the original value. FTIR spectra of the precipitates after DIC addition showed vibration peaks of the polymer and a variable intensity of the carbonate vibrations that were more prominent at lower pH values (Figure 1F). We further investigated the pH-dependent dissolution of the condensates, as it suggests an interaction between the polymer−Ca condensates and the carbonate system that is decoupled from the precipitation of calcium carbonate.

Following the rapid DIC-induced turbidity loss, we monitored the onset of calcium carbonate formation in the system. At all pH conditions, the final result was qualitatively similar, where fibrillar crystals developed during a time scale of days, and the condensates (if they were still present after DIC addition) disappeared (Figure 2A−C, see also Figure S6 for complete pH conditions). The forming crystals were of calcite, as determined by powder X-ray diffraction (PXRD) analyses of the sample (Figure 2B). The calcite crystals contain about 5% of organic content as determined with thermogravimetric analysis (TGA) and had a significant degree of short-range disorder as determined by FTIR "grinding curves" (Figure 2E,F).

https://doi.org/10.1021/acs.chemmater.5c03138
Chem. Mater. 2026, 38, 950−960

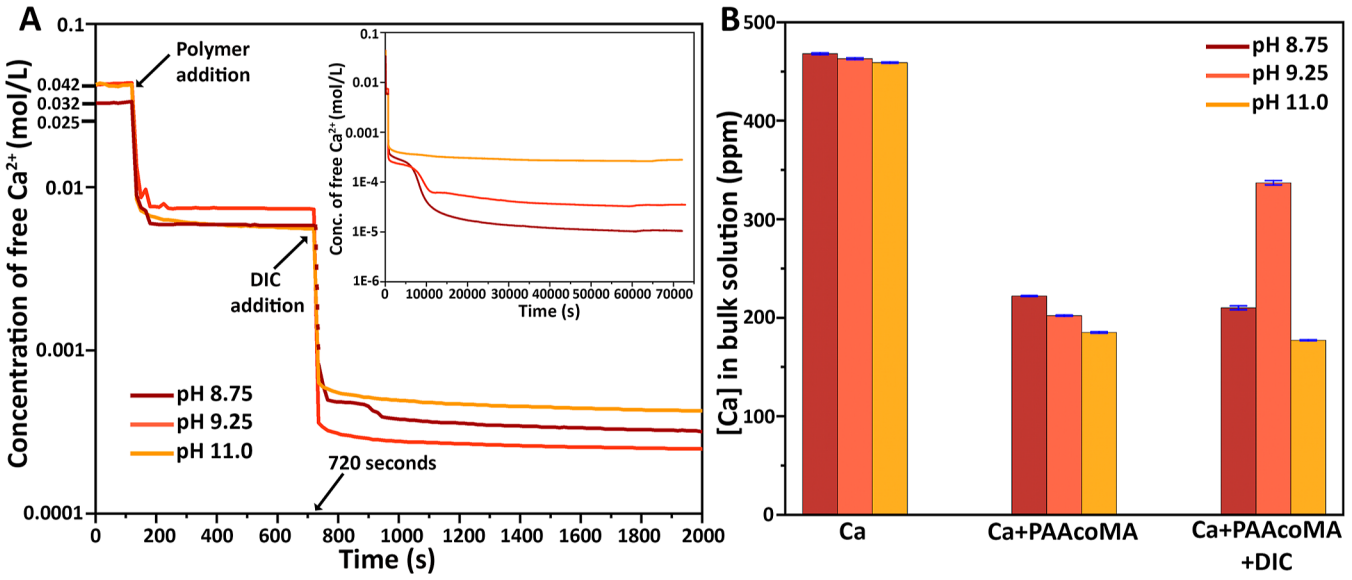

Figure 3. (A) Potentiometric measurement curves of Ca^{2+} concentrations along the reactions at different pH conditions. The inset shows the reaction time up to 20 h. The arrows indicate the addition of different components. The arrow pointing at 720 s indicates that the free Ca^{2+} concentration from then on can be considered quantitatively, as the calibration of the calcium ion-selective electrode matched these experimental conditions in terms of ionic strength. For pH 8.75, the whole experiment was performed in two steps, and the dotted line is used to connect the two data points at 720 s (see the Experimental Section for details). (B) ICP-OES data quantifying the total concentration of Ca in the supernatant at different stages of the mineralization reaction at three different pH conditions.

These observations reveal a 2-fold effect of pH on calcite crystallization in this system: kinetics, and yield. Even though the nominal concentrations of calcium and carbonate ions were identical at all pH values, hence supersaturation was similar across experiments, the kinetics of the reactions were very different (Figure 2D). At the basic pH values, it took over a week for all condensates to give way to the crystals, whereas at the lower pH values, the crystallization was completed in less than 2 days, with the fastest kinetics observed at pH 9.25, where the condensates disappeared upon DIC introduction. The yield of the reaction was also pH-dependent; as in the lower pH values, some of the bicarbonate ions converted into carbonate, allowing higher yield (Figure 2G). However, this trend was similar to that observed in polymer-free reactions, even though the substantial calcium complexation by the polymer reduced the amount of products. Overall, the effect of the polymer on calcium carbonate crystallization is mediated through the pH-dependent dissolution of the polymer−Ca condensates that dissolve rapidly around pH 9.25, leading to faster kinetics of crystallization at this pH range even though the thermodynamic driving force was similar.

From the previous observations, it appears that the main effect of PAAcoMA on calcite formation is via its reversible condensation with Ca^{2+} ions. Therefore, we investigated the origin of the pH-dependent condensate dissolution after DIC addition. It is clear that this is not a direct effect of pH, as the PAAcoMA−Ca condensates form at all pH values (Figure 1D), nor the result of the protonation degree of the polymer, as the carboxylic acid residues are mostly deprotonated at all pH values (Figure S4). These observations imply a direct interaction of the carbonate system with PAAcoMA−Ca condensates.

To understand the conditions in bulk solution along the different stages of the reaction, we conducted potentiometric experiments with a Ca^{2+} ion-selective electrode.[42] Ca^{2+} concentration over time was measured as the reaction proceeded (Figure 3A). In accordance with the turbidity observations, Ca^{2+} concentration directly drops upon addition of the polymer at all pH values (after 120 s in Figure 3A). When the DIC was introduced to the system at 720 s another drop was observed at all pH values. This observation seems to contrast with the apparent decrease in turbidity that is seen at pH 9.25 (and partially at pH 8.75), indicating that the dissolution of the PAAcoMA−Ca condensates does not result in free Ca^{2+} ions in solution but rather gives rise to a much more potent binding of Ca^{2+} with the DIC species. In fact, the drop in Ca^{2+} concentration is largest for pH 9.25, followed by pH 8.75 and pH 11, which inversely correlates with the observed turbidity behavior (cf. Figure 1E). The potentiometric data thus indicate that at pH 9.25, the strongest Ca^{2+}-binding occurs upon DIC addition to the PAAcoMA−Ca condensates. Therefore, the apparent discrepancy between the turbidity and potentiometric experiments is actually different sides of the same phenomenon. Namely, pH-dependent interactions of the carbonate species with Ca^{2+} ions, which are most effective around pH 9.25, drive the dissolution of the condensates for alternative interactions with the DIC. Even though the interactions of the Ca^{2+} ions with the DIC are stronger than with the polymer at all pH values, the data suggest that the species formed upon DIC addition are significantly smaller than the coacervates and are thus essentially invisible in the turbidity measurements. The last stage in the potentiometric experiment (inset in Figure 3A) records the long-term decrease in Ca^{2+} concentration that follows calcite crystallization. Here the different pH conditions follow the expected trend as in the total yield (Figure 2G), even though the pH 11 experiment did not reach the point of calcite crystallization (which did not occur within 20 h at this pH).

We complemented the potentiometric experiments with quantification of the total amount of Ca in the solution phase using ICP-OES. After each stage in the experiment, the

https://doi.org/10.1021/acs.chemmater.5c03138
Chem. Mater. 2026, 38, 950−960

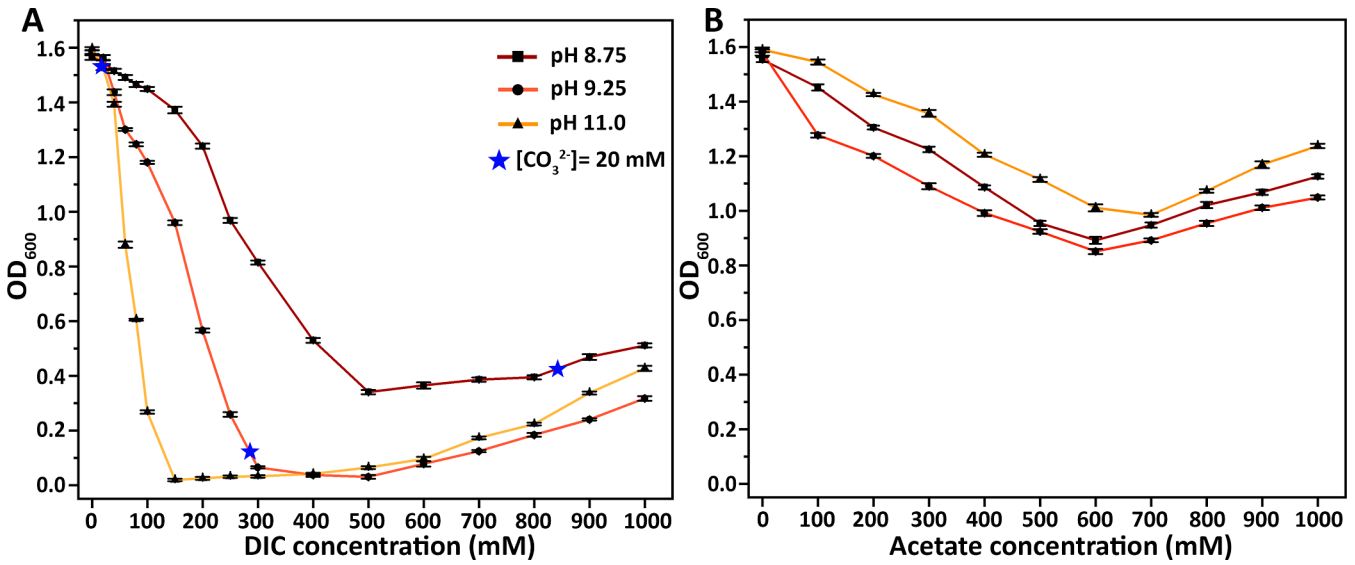

Figure 4. (A) Turbidity values of the PAAcoMA−Ca solution directly after the addition of various DIC solution concentrations, at three pH values. (B) Turbidity values of the PAAcoMA−Ca solution after the addition of sodium acetate solution at various concentrations, at three pH values.

precipitates were separated with centrifugation, and the Ca content in the supernatant was measured (Figure 3B). This analysis gives a trend that mirrors the turbidity measurements, where Ca content decreases upon polymer addition due to the sequestration in the condensates, and after DIC addition, the experiment at pH 9.25 shows a significant increase in Ca content. Altogether, these observations show a consistent view that DIC introduction induces the dissolution of condensates because they form other, higher-affinity and nonturbid species with Ca, and this binding efficiency is pH-dependent.

We investigated the relative roles of carbonate and bicarbonate ions by modifying the design of the DIC solutions. In the modified experiments, the pH and the ratio between carbonate and bicarbonate were kept constant while changing the total DIC concentrations. We monitored turbidity loss at these conditions and observed that at the entire pH range, DIC addition leads to concentration-dependent turbidity loss (Figure 4A). This behavior suggests that the carbonate species compete with the polymer molecules for the interactions with Ca^{2+} ions, and the presence of more carbonate species releases more calcium into calcium carbonate species until, at very high DIC concentrations, a recurrent increase in turbidity is measured again. Importantly, the concentration-dependent turbidity loss is more effective for carbonate-rich conditions (pH 11), over bicarbonate-rich conditions (pH 8.75). Highlighting the conditions of 20 mM carbonate concentrations at variable DIC and pH (Figure 4A—blue stars) mirrors the previous observations, recapitulating the dominant coacervate dissolution at pH 9.25.

The chemical similarity between the carbonate species and the carboxylic acid residues of the polymer led us to investigate another member of this family of molecules, the acetate ion, which, similarly to the carboxylic acid, has only one charged state. Indeed, also acetate yields a concentration-dependent turbidity loss, even though its magnitude is less than the carbonate system (Figure 4B). Overall, competitive interactions between carbonates and carboxylates underlie the balance between calcium ions that are bound in the polymer condensates, free in solution, or bound to DIC. This, in turn, affects the supersaturation in the dilute phase and the crystallization of calcium carbonate.

We investigated whether the in vitro observations of the effects of carbonate on the PAAcoMA−Ca coacervates can be recapitulated in biological systems. For this, we used the established model system of base plates and coccolith-associated polysaccharides (CAPs), extracted from coccoliths of the species *Pleurochrysis carterae*, which in the presence of Ca^{2+} ions form a calcium-rich dense phase on the base plate periphery (Figure 5A).[36,38,39] We note that previously, the CAP solution was used in its original, mildly acidic pH. In this pH, the formation of the dense phase is detected on the base plate periphery (Figure 5B,C).

We adjusted the pH of both the base plate and CAP solutions to the values tested in the PAAcoMA experiments. At all these pH values, we observed the formation of the CAP-mediated dense phase on the base plate peripheries (Figure 5D−F), similar to the previous observations at acidic pH. This is similar to pH insensitive PAAcoMA−Ca condensation (Figure 1D). Next, we added a DIC solution with a carbonate concentration comparable to that of the Ca^{2+} ions and CAPs. In the basic pH values, the dense phase persisted, as previously reported for experiments that induced calcite formation on the base plates.[38] Importantly, at the lower pH values, the dense phase disappeared (Figure 5G−I), and the same behavior was observed in the PAAcoMA case (Figure 1E). Additionally, increasing the DIC concentration at pH 11 caused the dissolution of the dense phase (Figure 5I), showing behavior similar to that shown in Figure 4A and further strengthening the similarities between the biological and synthetic systems.

DISCUSSION

The reported observations of the PAAcoMA−Ca-CO_3 system illustrate a new role for negatively charged macromolecules in calcium carbonate crystallization, which is distinct from the role of stabilizing metastable amorphous precursors. This is important, as the PILP concept has been used rather freely for any polymer-rich calcium carbonate formation, bringing some contradictory observations from different systems. For example, the liquid nature of the PILP,[43] its transformation

https://doi.org/10.1021/acs.chemmater.5c03138
Chem. Mater. 2026, 38, 950−960

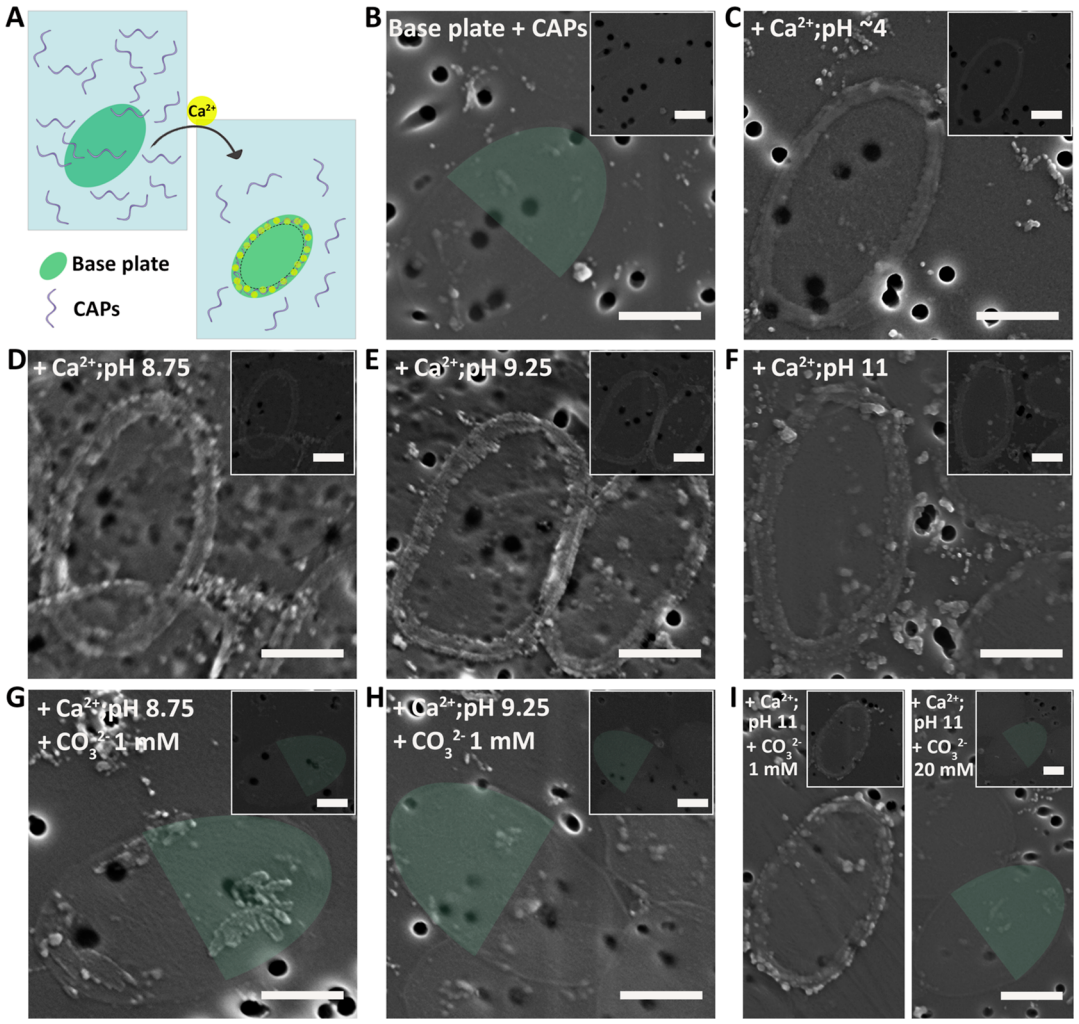

Figure 5. (A) Extracted base plate and CAPs associate in the presence of calcium ions to form a dense phase at the base plate periphery. (B–I) SEM images of dried samples on a supporting membrane. Insets show the corresponding backscattered electron detector images. When only base plate and CAPs are present (B), no dense phase is observed. Adding calcium ions to the solution (C) induces the formation of the coacervate at the base plate periphery. Similar observations are seen at more basic pH values (D–F). However, adding a DIC solution results in the disappearance of the dense phase at lower pH values or at higher DIC concentrations (G–I). Half of a base plate is artificially colored for better visualization in cases where no dense phase is present. Scale bars are 500 nm.

pathway,[44] and the formation process.[45,46] We propose that there is a need for tailored mechanistic and chemical characterization of each system that combines polymers and calcium carbonates because this is a family of very different phenomena.

In the current work, the substantial effect of the PAAcoMA–Ca condensates was to release calcium ions to the surrounding bulk solution upon carbonate introduction and, by this, to affect the kinetics of the crystallization process. This behavior is different from that of the related polymer PAA, which forms liquid condensates with calcium ions that transform to transient ACC in the presence of carbonate.[26] The denser charge density of PAAcoMA makes the condensates solid-like and prevents carbonate from interacting with them directly. This leads to an important difference; in the PAAcoMA system, calcium carbonate grows from the dilute phase, and the dense phase is not a preferred environment for crystallization, as was the case with PAA. The potentiometric experiments of free Ca^{2+} (Figure 3A) complement the turbidity and ICP observations of the Ca content in the precipitates and supernatant, respectively (Figures 3B and 1E). The emerging picture is of competition between the binding affinity for Ca^{2+} of the polymer and DIC.[47] At all pH values, the DIC species are strong binders of Ca^{2+} as Ca-concentration decreases, but only around pH 9.25 their binding is strong enough to induce the dissolution of the PAAcoMA–Ca condensates (Figure 3A), due to thermodynamic or kinetic reasons, or both. It will be interesting to examine the nature of the complexes that form in this system after condensate dissolution and see how the crystallization process compares to similar systems with less concentrated components.

This specificity of the interactions between different polymers and calcium carbonate means that in each system it is important not only to account for the properties of the polymer but also to monitor the state of the carbonate system. In the current system, this interaction gives rise to a counterintuitive behavior where lower pH values, which are usually associated with lower supersaturation, yield faster crystallization kinetics due to the increase of available Ca. This is in accordance with recent studies that highlight the influence of bicarbonate on the pathway of calcium carbonate crystallization.[48−50] This influence should be more profoundly

https://doi.org/10.1021/acs.chemmater.5c03138
Chem. Mater. 2026, 38, 950−960

studied, as it is reasonable that in biological processes, the pH is only mildly basic and can allow very high concentration of bicarbonate relative to carbonate. In addition, bicarbonate transporters are the preferred cellular machinery to deliver carbonate species for mineralization,[51] further emphasizing the importance of understanding the influence of bicarbonate on the reaction.

The similar carbonate-induced dissolution of the CAPs condensates that form on the coccolith base plate (Figure 5) points to a possible pathway that is used in the formation of coccoliths. It was suggested that CAPs function as calcium carriers that bring highly concentrated calcium to the site of crystallization,[52] but it is still unclear how, from such a crowded environment, the rhombohedral calcite crystals of the coccoliths nucleate and grow.[34,53] It is possible that the trigger for crystallization is a bicarbonate flux directed to the base plate. Such change in carbonate chemistry in the coccolith vesicle can induce both the observed dissolution of the condensates to release calcium ions,[28,29] and calcite formation. Altogether, even though many calcium carbonate biominerals are characterized by negatively charged macromolecules, each system can have its own unique behavior, and the release of calcium for crystallization may appear as an important factor.[54]

CONCLUSION

Negatively charged polymers can have various effects on the precipitation of calcium carbonate, which are collectively termed PILP. In the case of PAAcoMA, as well as biogenic CAPs, the polymer molecules complex calcium ions in solid-like condensates that sequester a portion of the available calcium from the solution. Upon the introduction of carbonate to the solution, calcium carbonate forms without the evidence of an immediate precursor phase. The presence of the carbonate and bicarbonate ions causes the dissolution of the polymer−Ca condensates, increasing the concentration of available calcium carbonate and thus accelerating the kinetics of crystallization. The dissolution of the condensates is driven by the competitive binding of carbonates and carboxylic acid residues. This behavior can explain the role of CAPs in coccolith formation and might also be relevant for other biomineralization processes.

EXPERIMENTAL SECTION

Reagents

Calcium chloride dihydrate (ACS reagent, ≥99%), sodium carbonate anhydrous (EMSURE), sodium bicarbonate (ACS reagent, ≥99.7%), and poly(acrylic acid-co-maleic acid) (Mw ∼ 3000 kDa, 50 wt % in H_2O), were all purchased from Sigma-Aldrich and used without any further purification. Glacial acetic acid, min. 99.95% anhydrous was purchased from Biolab Chemicals. Milli-Q water (resistivity: 18.2 MΩ·cm at 25 °C) was used for solution preparation. For pH adjustments, 1 M HCl and 1 M NaOH solutions were used. For balancing ionic strength, a freshly prepared 5 M NaCl solution was used.

Synthesis of PAAcoMA−Ca-CO_3

The concentration of the polymer was calculated in terms of the total number of acid groups (−COOH) in each monomer unit, which is 3, and the total number of monomer units in the polymer. Therefore, the concentration of the purchased solution was calculated to be 10 M. For our experiments, we prepared a stock solution of 540 mM by dilution with 1 M NaOH to adjust the pH of the solution to 8.5. $CaCl_2 2H_2O$ stock solution of 1 M in Milli-Q water was prepared. DIC solutions of 1.15 M at different pH values were prepared by mixing $NaHCO_3$ and Na_2CO_3 in the required ratios.

For mixing experiments, the reactants were adjusted to the predetermined pH and added in the right amounts to result in concentrations of 50 and 25 mM for PAAcoMA and Ca^{2+}, respectively. The final volume of a typical reaction was completed to 3 mL with the right amount of Milli-Q water (pH adjusted to the required pH) and the required volume of DIC or acetate solution. The pH of the resulting solution was monitored with time; there was no significant change at any step of the experiment. The solution tubes were constantly rotated at a moderate spinning rate in order to maintain a homogeneous chemical environment during the course of the reaction.

The resulting precipitate was observed either in the native form (optical microscope, turbidity measurements) or in the powdered form upon washing and lyophilization. A typical washing procedure of the samples involved centrifugation at 15,000 *g* for 2 min, followed by decantation of the liquid part. The pellets were resuspended in fresh Milli-Q water after every round. The process was repeated two times to remove any unreacted phases. The washed pellets were lyophilized to obtain the samples as dried powders.

Synthesis of PAAcoMA−Ca-Acetate

Sodium acetate stock solution, 1.5 M, of the desired pH, was prepared by adding the required amount of NaOH solution to 1 mL of glacial acetic acid. The experiments were performed in the same way as described above for CO_3.

PAAcoMA Titration for Protonation Determination

The titration was performed to determine the degree of ionization of the polymer with a pH. A titration set-up was made, and the pH was measured with a pH meter (Eutec pH 700). The titrate solution of PAAcoMA (50 mM, 10 mL) had an initial pH of 2 and was titrated with NaOH (1 M). The pH values were recorded with stepwise addition (5 μL) of NaOH. The exact titration points were resolved from the first-order derivative of the titration curve. The first titration point indicates the start of ionization of PAAcoMA, and the final point refers to its complete ionization (100%).

Extraction of Coccolith-Associated Polysaccharides and Base Plates

CAPs and base plates were extracted from *P. carterae* (CCMP645) cells using a published protocol.[36,39] After the cells were harvested, cellular material was separated from coccoliths using density gradient centrifugation with Percoll (GE Healthcare, Germany). The coccolith pellet was then rinsed multiple times with Milli-Q water. Base plates and CAPs were then released by dissolving the coccolith calcite with 0.5 M EDTA at pH 8. The organic material was desalted by five rounds of dialysis against Milli-Q water using cellulose dialysis tubes with a 14 kDa cutoff (Sigma-Aldrich). After dialysis, solutions were separated into the soluble CAPs fraction and the insoluble base plates through centrifugation at 20,000*g* for 15 min. The base plate-containing pellet was resuspended in 1 mL of pure water, and the supernatant containing the CAPs fraction was collected in a different 1 mL tube. The CAPs concentration used for experiments was the one that resulted from the extraction of 50 mL of stationary state cell culture and collected in 1 mL. The molarity of carboxylic groups of CAPs was estimated to be ∼1.7 mM.[39]

Experiments with CAPs and Base Plate

Five microliter portion of base plate solution was added to CAPs solution, this was followed by the addition of Ca^{2+} and NaOH in order to attain the desired pH. The resulting solution has CAPs concentration of ∼0.9× (1.5 mM) and [Ca^{2+}] 1 mM. In DIC-added experiments, an HCO_3^-/CO_3^{2-} solution was added to attain the desired concentration values of [CO_3^{2-}].

Turbidity Measurements

To quantify the turbidity, optical density measurements were conducted at 600 nm on an Ultraspec 2100 pro UV/visible spectrophotometer.

https://doi.org/10.1021/acs.chemmater.5c03138
Chem. Mater. 2026, 38, 950−960

Optical Microscope Imaging

Fifteen microliter portion of the solution sample was pipetted on a glass slide, and a coverslip was placed over it. The samples were observed in a Nikon Upright Optical Microscope, Eclipse Ni-U.

Scanning Electron Microscope

The lyophilized samples were mounted on SEM stubs, coated with 5 nm iridium (Compact Coating Unit, CCU-010, Safematic), and imaged using SEM (Sigma 500, Zeiss) at a working distance of 2.5 mm with 3 kV using the in-lens detector. For the experiments with CAPs, the samples were directly pipetted onto a 0.1 μm Nanopore track etch membrane (Whatman, 13 mm) and dried using vacuum filtration and then mounted on SEM stubs with the help of carbon tape. Here, the samples were coated with 5 nm of carbon (Compact Coating Unit, CCU-010, Safematic) and imaged in an SEM (Ultra 55 FEG, Zeiss) at a working distance of 2 mm with 2 kV using either the in-lens or in-lens detector for backscattered electrons. The energy-selective backscattered detector grid voltage was set to 700 V.

Fourier Transform Infrared Spectroscopy

The lyophilized samples were measured on a Thermo Scientific Nicolet iS5 Fourier transform infrared (FTIR) spectrometer by preparing KBr pellets using an agate mortar and pestle, and then the mixture was pressed into a 7 mm pellet with a hand press.

Grinding Curve

The samples were analyzed by FTIR in transmission mode to compare them to calcite standards obtained with the grinding curve method.[41] This method allows one to determine the degree of short-range atomic order of crystals. The repeated grinding of the sample containing KBr pellets affects peak widths and relative heights of mineral samples involving calcite and apatite. It is well established that by normalizing the ν_2 and ν_4 peak heights relative to the height of the ν_3 peak, a consistent trend emerges that decouples the effect of grinding from the intrinsic order in the material. In this work, three different PAAcoMA−Ca-CO_3 samples synthesized at pH 8.75 after complete crystallization were analyzed; all three samples produced similar trends. FTIR spectra were processed using OMNIC v. 9.13 and Macros Basic v. 10, and the normalized ν_2 and ν_4 absorptions of calcite were compared with published grinding curves of calcite standards.[41]

Thermogravimetric Analysis

Analyses of the lyophilized samples were performed on an SDT Q600, TA Instruments, USA. Analyses were performed under an air atmosphere (injection rate of 100 mL/min) with a heating rate of 10 K/min. A typical measurement involved 4 mg of a lyophilized sample.

Nuclear Magnetic Resonance Spectroscopy

All NMR experiments were recorded on a 9.4 T (400.35 MHz) Bruker AVANCE NEO spectrometer at 298 K. The chemical shifts (δ) are given in parts per million relative to a residual solvent resonance (4.7 ppm for D_2O).

Both 1D and 2D diffusion experiments were performed on an NMR spectrometer equipped with a 50 gauss/cm Z gradient system. The stimulated echo sequence with bipolar smoothed square (SMSQ.10.100) gradients was used. The 1D diffusion experiment was used to remove fast diffusing compounds from the ^{1}H spectrum (mostly impurities and solvents). To achieve that, a total of 5 ms gradient length was used with 100% power and a 100 ms diffusion time. The experiment was performed with a 5 s recycle delay and 64 scans. For the pseudo 2D diffusion experiments, used to extract the diffusion coefficients of both the monomer and the polymers, the gradients were incremented from 2% to 98% in 10 linear steps, and 32 scans were acquired for each gradient. The gradient duration was 3 ms, and the diffusion time was 100 ms. All diffusion coefficients were calculated from the NMR data by using a diffusion coefficient reference of 2.0×10^{-5} cm^2/s for the water signal. The approximate molecular weight of the polymer was extracted from the diffusion data by assuming an almost linear structure for the polymer; thus, the ratio between the diffusion coefficients of the monomer and the polymer is approximately scaled to the root square of their respective molecular weights.

The ^{1}H−^{13}C HSQC experiment was acquired with a spectral width of 16 ppm for ^{1}H and 200 ppm for the ^{13}C, a matrix of 2 K × 256 (zero filled to 4 K × 1 K), 1.5 s recycle delay, and 32 scans.

Dynamic Light Scattering

A Zetasizer (Nano ZSP, Malvern Instruments, United Kingdom) equipped with a 633 nm laser was used to measure particle sizes in real time. The particle sizes were determined by the intensity distribution and presented as the average values of three replicate measurements.

Powder X-ray Diffraction

The XRD patterns of the lyophilized samples were obtained from STOE STADI P in the transmission mode with Cu-Kα (λ = 1.54060 Å) source and MYTHEN2 R detector. The data were obtained in the 2θ range of 2−80°, with the acquisition parameter set as the Time/PSD step = 10 s.

Potentiometric Measurement Experiments

Calcium concentration measurements were performed using an autotitrator (Metrohm OMNIS) operated via OMNIS software (Version 4.2.0). The titration apparatus comprised two dosing units (the OMNIS Titrator and OMNIS Dosing Module) for the precise addition of NaOH (0.1 M, Roth 6783.1) and $CaCl_2$ (0.2 M, VWR Chemicals 1,90,464 K) solutions. This $CaCl_2$ solution was used only in the calibration experiments.

Measurements of pH and free calcium−ion potentials were conducted using a pH electrode (Metrohm 6.0256.100) and a calcium−ion-selective electrode (Ca-ISE, Metrohm No. 6.0508.110). The pH electrode has an inner Ag/AgCl reference electrode, the electrolyte of which is a 3 M KCl solution (Merck) and it was calibrated with buffers at pH values of 4.01, 7.00, and 9.21 (Mettler-Toledo 51 302 070, 51 302 047, and 51 302 070). The calcium electrode was calibrated daily to ensure precise and accurate measurements.

Calibration Experiments

NaCl (for analysis, PanReac 131659.1211) was added to 30.00 mL of degassed ultrapure water to match the ionic strength of the experimental conditions: 0.125 M (low ionic strength), 1 M (high ionic strength) for pH 8.75, 0.45 M for pH 9.25, and 0.19 M for pH 11. After adjusting the pH to the target value, calibration was initiated by adding a $CaCl_2$ solution (0.2 M) at a rate of 0.01 mL/min. The electrodes were calibrated up to a Ca^{2+} concentration of 4 mM for every experiment. The changes in the measured potential of the Ca-ISE were then correlated with changes in the free calcium ion concentration. By adjusting the ionic strength, we are able to determine the concentration of Ca^{2+} ions rather than their activity, as would occur if the experiments were performed in pure water [42]. The pH was maintained constant through the automatic titration of the NaOH solution (0.1 M). Calibrations were concluded after 1 h, and the maximum potentials attained were 25.8 and 24.2 mV for pH 8.75, low ionic strength and high ionic strength, respectively; 32.4 mV for pH 9.25 and 26.1 mV for pH 11.

PAAcoMA−Ca-CO_3 Potentiometric Measurement Experiments

The calcium concentration and transformation measurements were conducted in a solution with a final total volume of 30.00 mL, constituted of aqueous solutions of PAAcoMA (50 mM final concentration), $CaCl_2$ (25 mM final concentration), and DIC solutions at different pHs (8.75, 9.25, and 11), where the final [CO_3^{2-}] was 20 mM. Thus, a larger amount of total DIC was added at lower than at higher pH, as the fraction of [CO_3^{2-}] increases with increasing pH. Each experiment started with 0.75 mL of $CaCl_2$ solution and a certain volume of Milli-Q water, followed by the polymer addition (2.8 mL) and DIC (different volumes at different pH). The volume of water was calculated in each case to make the total volume equal to 30 mL. It is to be noted that for pH 8.75, a huge

https://doi.org/10.1021/acs.chemmater.5c03138
Chem. Mater. 2026, 38, 950−960

fraction of the total volume of 30 mL was contributed by DIC, i.e., 25 mL. As a result, it was not possible to do the complete reaction in one experiment, as otherwise the Ca^{2+}-electrode would not immerse in solution, and this would prevent us from obtaining the measurement until DIC addition at 720 s. To compensate for this, the reaction was done in two steps, one where the Ca^{2+} potential was measured only for the PAAcoMA and Ca^{2+} in solution for 720 s (calibration experiment was done separately for the corresponding ionic strength, referred to as low ionic strength). In the second reaction, the Ca^{2+} potential measurement was obtained for the solution with all of the components (referred to as high ionic strength). A dotted line was used to connect the two separate curves for pH 8.75 in Figure 3B.

The initial values of Ca^{2+} concentration and volume for the different pHs were: for pH 8.75 (low ionic strength), 27.6 mM and 27.2 mL; for pH 9.25, 40.3 mM and 18.62 mL; and for pH 11, 28.4 mM and 26.44 mL. For pH 8.75 (high ionic strength), we do not have these initial values, as, due to volume restrictions, we already started the measurements with a certain amount of DIC in solution. The pH (8.75, 9.25, and 11.0) of the calcium solution was adjusted prior to the commencement of the measurement using HCl (0.1 M) and NaOH (0.1 M) solutions. During the experiment, 0.1 M NaOH was automatically added to maintain a constant pH. For every experiment, the polymer solution was added to the Ca^{2+} aqueous solution 120 s after beginning the measurement. The initial concentration of the polymer in each solution was 50 mM for pH 8.75 (low ionic strength), undeterminable for the high ionic strength (as explained above); 70 mM for pH 9.25, and 51.5 mM for pH 11. Subsequently, changes in pH, free calcium ion concentration, and the amount of NaOH added over time were recorded. After an additional 600 s, the DIC solution was added. The concentration of the stock solutions was 1 M in each case; however, to match 20 mM $[CO_3^{2-}]$ at every pH, different volumes were added, and as a result, the DIC concentrations in the final solution (30 mL) would vary at different pH. The volume of DIC added and their concentration in solution at pH 8.75 were 25 mL and 833 mM; at pH 9.25, they were 8.58 mL and 286 mM; and at pH 11, they were 750 mL and 25 mM. The measurements were run for 20 h for more insights into the reaction mechanism via the changes in free Ca^{2+} concentration over time.

Inductively Coupled Plasma Optical Emission Spectroscopy

ICP-OES analysis to determine the concentration of Ca at different stages of the mineralization reaction was performed on a Spectro Arcos spectrometer. Samples and calibration solutions were aqueous solutions in Milli-Q water and dissolved in 2.5% HNO_3 containing 20 ppm indium (diluted from Indium ICP standard solution, 1000 ppm purchased from Carl Roth). Calibration solutions for five-point calibration (0−750 ppm) were prepared from Ca standard solutions (1000 ppm ICP standard solutions purchased from Carl Roth). Experimental samples at three different pH conditions: 8.75, 9.25, and 11 were analyzed. For each pH condition, three different stages of the reaction were subjected to analyses, only Ca; Ca + PAAcoMA and Ca + PAAcoMA + DIC. To achieve statistical precision, each sample was analyzed in triplicate. The samples forming coacervates (containing PAAcoMA and also upon DIC addition) were centrifuged, and only the supernatants were subjected to analyses to determine the concentration of dissolved Ca. The samples were diluted to half the original concentration with 2.5% HNO_3.

■ ASSOCIATED CONTENT

● Supporting Information

The Supporting Information is available free of charge at https://pubs.acs.org/doi/10.1021/acs.chemmater.5c03138.

Additional ^1H and ^{13}C NMR data, turbidity measurements, degree of ionization of the polymer, FT-IR spectra, optical microscopy, and SEM images (PDF)

■ AUTHOR INFORMATION

Corresponding Author

Assaf Gal − *Department of Plant and Environmental Sciences, Weizmann Institute of Science, Rehovot 7610001, Israel;* orcid.org/0000-0003-1488-1227; Email: assaf.gal@weizmann.ac.il

Authors

Debojit Paul − *Department of Plant and Environmental Sciences, Weizmann Institute of Science, Rehovot 7610001, Israel; Institute of Inorganic Chemistry, Leibniz University Hannover, Hannover 30167, Germany*

Oliver Jeske − *Institute of Inorganic Chemistry, Leibniz University Hannover, Hannover 30167, Germany*

Oksana Yanshyna − *Department of Plant and Environmental Sciences, Weizmann Institute of Science, Rehovot 7610001, Israel*

Liat Avram − *Department of Chemical Research Support, Weizmann Institute of Science, Rehovot 7610001, Israel;* orcid.org/0000-0001-6535-3470

Denis Gebauer − *Institute of Inorganic Chemistry, Leibniz University Hannover, Hannover 30167, Germany; Department of Chemistry, University of Konstanz, Konstanz 78464, Germany;* orcid.org/0000-0003-1612-051X

Complete contact information is available at: https://pubs.acs.org/10.1021/acs.chemmater.5c03138

Notes

The authors declare no competing financial interest.

■ ACKNOWLEDGMENTS

We acknowledge Protap Biswas and Leilah Otikovs, Weizmann Institute of Science, for their experimental guidance. This research was supported by an award from the US Office of Naval Research Global and US Army Research Laboratory (N62909-23-1-2026).

■ REFERENCES

(1) Deng, Z.; Jia, Z.; Li, L. Biomineralized Materials as Model Systems for Structural Composites: Intracrystalline Structural Features and Their Strengthening and Toughening Mechanisms. *Adv. Sci.* **2022**, *9* (14), 2103524.

(2) Yao, S.; Jin, B.; Liu, Z.; Shao, C.; Zhao, R.; Wang, X.; Tang, R. Biomineralization From Material Tactics to Biological Strategy. *Adv. Mater.* **2017**, *29* (14), 1605903.

(3) Aizenberg, J.; Hanson, J.; Koetzle, T. F.; Weiner, S.; Addadi, L. Control of Macromolecule Distribution within Synthetic and Biogenic Single Calcite Crystals. *J. Am. Chem. Soc.* **1997**, *119* (5), 881−886.

(4) Weiner, S.; Traub, W. Macromolecules in Mollusc Shells and Their Functions in Biomineralization. *Philos. Trans. R. Soc. Lond. B Biol. Sci.* **1984**, *304* (1121), 425−434.

(5) Mao, L. B.; Gao, H. L.; Yao, H. B.; Liu, L.; Cölfen, H.; Liu, G.; Chen, S. M.; Li, S. K.; Yan, Y. X.; Liu, Y. Y.; Yu, S. H.; Yu, S. H. Synthetic Nacre by Predesigned Matrix-Directed Mineralization. *Science* **2016**, *354* (6308), 107−110.

(6) Robin, M.; Djediat, C.; Bardouil, A.; Baccile, N.; Chareyron, C.; Zizak, I.; Fratzl, P.; Selmane, M.; Haye, B.; Genois, I.; Krafft, J. M.; Costentin, G.; Azaïs, T.; Artzner, F.; Giraud-Guille, M. M.; Zaslansky, P.; Nassif, N. Acidic Osteoid Templates the Plywood Structure of Bone Tissue. *Adv. Sci.* **2023**, *11*, 2304454.

(7) Gotliv, B.-A.; Kessler, N.; Sumerel, J. L.; Morse, D. E.; Tuross, N.; Addadi, L.; Weiner, S. Asprich: A Novel Aspartic Acid-Rich Protein Family from the Prismatic Shell Matrix of the Bivalve *Atrina Rigida*. *ChemBioChem* **2005**, *6* (2), 304−314.

(8) Suzuki, M.; Saruwatari, K.; Kogure, T.; Yamamoto, Y.; Nishimura, T.; Kato, T.; Nagasawa, H. An Acidic Matrix Protein, Pif, Is a Key Macromolecule for Nacre Formation. *Science* **2009**, *325* (5946), 1388−1390.
(9) Falini, G.; Albeck, S.; Weiner, S.; Addadi, L. Control of Aragonite or Calcite Polymorphism by Mollusk Shell Macromolecules. *Science* **1996**, *271* (5245), 67−69.
(10) Walker, C. E.; Heath, S.; Salmon, D. L.; Smirnoff, N.; Langer, G.; Taylor, A. R.; Brownlee, C.; Wheeler, G. L. An Extracellular Polysaccharide-Rich Organic Layer Contributes to Organization of the Coccosphere in Coccolithophores. *Front. Mar. Sci.* **2018**, *5*, 306.
(11) Arias, J. L.; Fernández, M. S. Polysaccharides and Proteoglycans in Calcium Carbonate-Based Biomineralization. *Chem. Rev.* **2008**, *108* (11), 4475−4482.
(12) Gebauer, D.; Wolf, S. E. Designing Solid Materials from Their Solute State: A Shift in Paradigms toward a Holistic Approach in Functional Materials Chemistry. *J. Am. Chem. Soc.* **2019**, *141* (11), 4490−4504.
(13) Gilbert, P. U. P. A.; Abrecht, M.; Frazer, B. H. The Organic-Mineral Interface in Biominerals. *Molecular Geomicrobiology*; De Gruyter, 2005; vol. *59*, pp 157−186.
(14) Asenath-Smith, E.; Li, H.; Keene, E. C.; Seh, Z. W.; Estroff, L. A. Crystal Growth of Calcium Carbonate in Hydrogels as a Model of Biomineralization. *Adv. Funct. Mater.* **2012**, *22* (14), 2891−2914.
(15) Addadi, L.; Raz, S.; Weiner, S. Taking Advantage of Disorder: Amorphous Calcium Carbonate and Its Roles in Biomineralization. *Adv. Mater.* **2003**, *15* (12), 959−970.
(16) Kim, Y.-Y.; Ganesan, K.; Yang, P.; Kulak, A. N.; Borukhin, S.; Pechook, S.; Ribeiro, L.; Kröger, R.; Eichhorn, S. J.; Armes, S. P.; Pokroy, B.; Meldrum, F. C. An Artificial Biomineral Formed by Incorporation of Copolymer Micelles in Calcite Crystals. *Nat. Mater.* **2011**, *10* (11), 890−896.
(17) De Yoreo, J. J.; Gilbert, P. U. P. A.; Sommerdijk, N. A. J. M.; Penn, R. L.; Whitelam, S.; Joester, D.; Zhang, H.; Rimer, J. D.; Navrotsky, A.; Banfield, J. F.; Wallace, A. F.; Michel, F. M.; Meldrum, F. C.; Cölfen, H.; Dove, P. M. Crystallization by Particle Attachment in Synthetic, Biogenic, and Geologic Environments. *Science* **2015**, *349* (6247), aaa6760.
(18) Gower, L. B.; Odom, D. J. Deposition of Calcium Carbonate Films by a Polymer-Induced Liquid-Precursor (PILP) Process. *J. Cryst. Growth* **2000**, *210* (4), 719−734.
(19) Gower, L. B. Biomimetic Model Systems for Investigating the Amorphous Precursor Pathway and Its Role in Biomineralization. *Chem. Rev.* **2008**, *108* (11), 4551−4627.
(20) Gruber, D.; Ruiz-Agudo, C.; Cölfen, H. Cationic Coacervates: Novel Phosphate Ionic Reservoir for the Mineralization of Calcium Phosphates. *ACS Biomater. Sci. Eng.* **2023**, *9* (4), 1791−1795.
(21) Rowland, A. T.; Cacace, D. N.; Pulati, N.; Gulley, M. L.; Keating, C. D. Bioinspired Mineralizing Microenvironments Generated by Liquid-Liquid Phase Coexistence. *Chem. Mater.* **2019**, *31* (24), 10243−10255.
(22) Liu, Z.; Shao, C.; Jin, B.; Zhang, Z.; Zhao, Y.; Xu, X.; Tang, R. Crosslinking Ionic Oligomers as Conformable Precursors to Calcium Carbonate. *Nature* **2019**, *574* (7778), 394−398.
(23) Avaro, J. T.; Wolf, S. L. P.; Hauser, K.; Gebauer, D. Stable Prenucleation Calcium Carbonate Clusters Define Liquid−Liquid Phase Separation. *Angew. Chem., Int. Ed.* **2020**, *59* (15), 6155−6159.
(24) Dai, S.; Xie, Z.; Wang, B.; Ye, R.; Ou, X.; Wang, C.; Yu, N.; Huang, C.; Zhao, J.; Cai, C.; Zhang, F.; Buratto, D.; Khan, T.; Qiao, Y.; Hua, Y.; Zhou, R.; Tian, B. An Inorganic Mineral-Based Protocell with Prebiotic Radiation Fitness. *Nat. Commun.* **2023**, *14* (1), 7699.
(25) Kuhrts, L.; Prévost, S.; Chevrier, D. M.; Pekker, P.; Spaeker, O.; Egglseder, M.; Baumgartner, J.; Pósfai, M.; Faivre, D. Wettability of Magnetite Nanoparticles Guides Growth from Stabilized Amorphous Ferrihydrite. *J. Am. Chem. Soc.* **2021**, *143* (29), 10963−10969.
(26) Paul, D.; Varsano, N.; Biswas, P.; Kaplan-Ashiri, I.; Aram, L.; Gal, A. Non-Stoichiometric Amorphous Calcium Carbonate Forms in Macromolecular Condensates via Interphase Diffusion. *Small* **2025**, *21* (10), 2411965.
(27) Stifler, C. A.; Killian, C. E.; Gilbert, P. U. P. A. Evidence for a Liquid Precursor to Biomineral Formation. *Cryst. Growth Des.* **2021**, *21* (12), 6635−6641.
(28) Bino, E.; Aram, L.; Paul, D.; Kadan, Y.; Clare, D.; Gilchrist, J. B.; Elad, N.; Gal, A. The Role of Macromolecular Condensates in the Regulation of Intracellular Calcium Transport for Coccolith Formation. *Adv. Funct. Mater.* **2024**, *35* (7), 2415344.
(29) Kadan, Y.; Tollervey, F.; Varsano, N.; Mahamid, J.; Gal, A. Intracellular Nanoscale Architecture as a Master Regulator of Calcium Carbonate Crystallization in Marine Microalgae. *Proc. Natl. Acad. Sci. U.S.A.* **2021**, *118* (46), No. e2025670118.
(30) Blondeau, M.; Sachse, M.; Boulogne, C.; Gillet, C.; Guigner, J.-M.; Skouri-Panet, F.; Poinsot, M.; Ferard, C.; Miot, J.; Benzerara, K. Amorphous Calcium Carbonate Granules Form Within an Intracellular Compartment in Calcifying Cyanobacteria. *Front. Microbiol.* **2018**, *9*, 1768.
(31) Li, J.; Liu, P.; Menguy, N.; Zhang, X.; Wang, J.; Benzerara, K.; Feng, L.; Sun, L.; Zheng, Y.; Meng, F.; Gu, L.; Leroy, E.; Hao, J.; Chu, X.; Pan, Y. Intracellular Silicification by Early-Branching Magnetotactic Bacteria. *Sci. Adv.* **2022**, *8* (19), No. eabn6045.
(32) Young, J. R. Biomineralization Within Vesicles: The Calcite of Coccoliths. *Rev. Mineral. Geochem.* **2003**, *54* (1), 189−215.
(33) Yin, X.; Ziegler, A.; Kelm, K.; Hoffmann, R.; Watermeyer, P.; Alexa, P.; Villinger, C.; Rupp, U.; Schlüter, L.; Reusch, T. B. H.; Griesshaber, E.; Walther, P.; Schmahl, W. W. Formation and Mosaicity of Coccolith Segment Calcite of the Marine Algae *Emiliania huxleyi*. *J. Phycol.* **2018**, *54* (1), 85−104.
(34) Avrahami, E. M.; Houben, L.; Aram, L.; Gal, A. Complex Morphologies of Biogenic Crystals Emerge from Anisotropic Growth of Symmetry-Related Facets. *Science* **2022**, *376* (6590), 312−316.
(35) Marsh, M. E. Coccolith Crystals of *Pleurochrysis carterae*: Crystallographic Faces, Organization, and Development. *Protoplasma* **1999**, *207* (1−2), 54−66.
(36) Gal, A.; Wirth, R.; Kopka, J.; Fratzl, P.; Faivre, D.; Scheffel, A. Macromolecular Recognition Directs Calcium Ions to Coccolith Mineralization Sites. *Science* **2016**, *353* (6299), 590−593.
(37) Marzec, B.; Walker, J. M.; Panagopoulou, M.; Jhons, Y.; Clare, D.; Wheeler, A.; Shaver, M. P.; Nudelman, F. Three-Dimensional Architecture and Surface Functionality of Coccolith Base Plates. *J. Struct. Biol.* **2019**, *208* (2), 127−136.
(38) Gal, A.; Wirth, R.; Barkay, Z.; Eliaz, N.; Scheffel, A.; Faivre, D. Templated and Self-Limiting Calcite Formation Directed by Coccolith Organic Macromolecules. *Chem. Commun.* **2017**, *53* (55), 7740−7743.
(39) Krounbi, L.; Hedderick, K.; Eyal, Z.; Aram, L.; Shimoni, E.; Estroff, L. A.; Gal, A. Surface-Induced Coacervation Facilitates Localized Precipitation of Mineral Precursors from Dilute Solutions. *Chem. Mater.* **2021**, *33* (10), 3534−3542.
(40) Banani, S. F.; Lee, H. O.; Hyman, A. A.; Rosen, M. K. Biomolecular Condensates: Organizers of Cellular Biochemistry. *Nat. Rev. Mol. Cell Biol.* **2017**, *18* (5), 285−298.
(41) Poduska, K. M.; Regev, L.; Boaretto, E.; Addadi, L.; Weiner, S.; Kronik, L.; Curtarolo, S. Decoupling Local Disorder and Optical Effects in Infrared Spectra: Differentiating between Calcites with Different Origins. *Adv. Mater.* **2011**, *23* (4), 550−554.
(42) Kellermeier, M.; Picker, A.; Kempter, A.; Cölfen, H.; Gebauer, D. A Straightforward Treatment of Activity in Aqueous $CaCO_3$ Solutions and the Consequences for Nucleation Theory. *Adv. Mater.* **2014**, *26* (5), 752−757.
(43) Shao, C.; Pan, H.; Tao, J.; Cho, K. R.; Tang, R.; Gower, L. B.; De Yoreo, J. J. Time Evolution of Moduli of a Polymer-Induced Liquid Precursor (PILP) of Calcium Carbonate. *Chem. Commun.* **2024**, *60* (29), 3950−3953.
(44) Xu, Y.; Tijssen, K. C. H.; Bomans, P. H. H.; Akiva, A.; Friedrich, H.; Kentgens, A. P. M.; Sommerdijk, N. A. J. M. Microscopic Structure of the Polymer-Induced Liquid Precursor for Calcium Carbonate. *Nat. Commun.* **2018**, *9* (1), 2582.
(45) Chen, J.; Gao, G.; Zhang, Z.; Sun, T.; Fu, Z.; Zou, Z. Nanocluster-Induced Liquid-like Precursor Formation and Crystal-

lization: In Situ Visualization and 3D Reconstruction. *J. Am. Chem. Soc.* **2025**, *147* (11), 9590−9600.
(46) Smeets, P. J. M.; Finney, A. R.; Habraken, W. J. E. M.; Nudelman, F.; Friedrich, H.; Laven, J.; De Yoreo, J. J.; Rodger, P. M.; Sommerdijk, N. A. J. M. A Classical View on Nonclassical Nucleation. *Proc. Natl. Acad. Sci. U.S.A.* **2017**, *114* (38), E7882−E7890.
(47) Gindele, M. B.; Malaszuk, K. K.; Peter, C.; Gebauer, D. On the Binding Mechanisms of Calcium Ions to Polycarboxylates: Effects of Molecular Weight, Side Chain, and Backbone Chemistry. *Langmuir* **2022**, *38* (47), 14409−14421.
(48) Jin, B.; Chen, Y.; Pyles, H.; Baer, M. D.; Legg, B. A.; Wang, Z.; Washton, N. M.; Mueller, K. T.; Baker, D.; Schenter, G. K.; Mundy, C. J.; De Yoreo, J. J. Formation, Chemical Evolution and Solidification of the Dense Liquid Phase of Calcium (Bi)Carbonate. *Nat. Mater.* **2024**, *24*, 125−132.
(49) Huang, Y.; Rao, A.; Huang, S.; Chang, C.; Drechsler, M.; Knaus, J.; Chan, J. C. C.; Raiteri, P.; Gale, J. D.; Gebauer, D. Uncovering the Role of Bicarbonate in Calcium Carbonate Formation at Near-Neutral PH. *Angew. Chem., Int. Ed.* **2021**, *60* (30), 16707−16713.
(50) Piaggi, P. M.; Gale, J. D.; Raiteri, P. Ab Initio Machine-Learning Simulation of Calcium Carbonate from Aqueous Solutions to the Solid State. *Proc. Natl. Acad. Sci. U.S.A.* **2025**, *122* (41), No. e2415663122.
(51) Kottmeier, D. M.; Chrachri, A.; Langer, G.; Helliwell, K. E.; Wheeler, G. L.; Brownlee, C. Reduced H^+ Channel Activity Disrupts PH Homeostasis and Calcification in Coccolithophores at Low Ocean PH. *Proc. Natl. Acad. Sci. U.S.A.* **2022**, *119* (19), No. e2118009119.
(52) Marsh, M. E. Polyanion-Mediated Mineralization—Assembly and Reorganization of Acidic Polysaccharides in the Golgi System of a Coccolithophorid Alga during Mineral Deposition. *Protoplasma* **1994**, *177* (3), 108−122.
(53) Avrahami, E. M.; Eyal, Z.; Varsano, N.; Zagoriy, I.; Mahamid, J.; Gal, A. Transport-Limited Growth of Coccolith Crystals. *Adv. Mater.* **2023**, *36* (11), 2309547.
(54) Namikawa, Y.; Zhu, L.; Lu, P.; Nagata, K.; Suzuki, M. Calcium dissociation with carbonate ions from Pf-SCP, Sarcoplasmic Calcium-binding Protein in *Pinctada fucata*, Contributes to Calcium Mineralization for Shell Formation. *Protein Sci.* **2025**, *34* (11), No. e70336.

https://doi.org/10.1021/acs.chemmater.5c03138
Chem. Mater. 2026, 38, 950−960